

Frequency stabilization of a 1621 nm laser to detect a transition in H_2^+ ions

L. Brusset^a

a. Mines Paris PSL + louis.brusset@etu.minesparis.psl.eu

Key words: Laser control ; ECDL ; Frequency comb ; Beat-note ; Feedback loop ; REFIMEVE

Abstract:

This paper focuses on the control of a 1621 nm semiconductor laser, which is useful for the detection of H_2^+ ions in Coulomb crystals, in the frame of the H_2^+ high resolution spectroscopy project developed at Kastler Brossel laboratory (LKB). It is locked on a frequency comb, which is locked on the REFIMEVE ultrastable signal broadcasted by SYRTE laboratory. We present a review of the laser characteristics and the experimental set up. The results show that it is possible to obtain a very precise frequency and an excellent signal-to-noise ratio, but there is room for improvement in the quality of the components used. A very precise 1621 nm laser source is obtained.

1 Introduction

The aim of this report is to present how to obtain a laser at a precise wavelength in order to induce an vibrational transition in a molecular ion. This work is part of a fundamental research project aimed at improving the accuracy of the measurement of $\mu_{pe} = m_p/m_e$, the ratio between the mass of the proton [1] and that of the electron [2]. This is an essential universal constant in quantum physics, playing a central role in understanding the fundamental laws governing interactions at the atomic scale. Until 1976 [3], research into μ_{pe} relied on spectroscopy of the molecular ion HD^+ (deuteron), but from 2001 onwards, it was demonstrated that spectroscopy of the H_2^+ ion offered a more direct approach [4], requiring a single measurement to determine μ_{pe} , compared with two for HD^+ .

The constant μ_{pe} is a fundamental constant of the universe, along with the fine structure constant α , the proton radius size r_p and the Rydberg constant R_∞ [5]. All four are involved in the calculation of ro-vibrational transitions. As in this equation combining relativistic corrections and dependence on μ_{pe} :

$$\nu = c \cdot R_\infty \cdot \left\{ \nu_{\text{NR}} \left(\frac{m_p}{m_e} \right) + f(\alpha) + f_{\text{FS}}(r_p) \right\}, \quad (1.1)$$

where ν_{NR} , f and f_{FS} are numerically known functions. Thus, increased precision on μ_{pe} enables complex atomic physics models to be refined. Currently known to an accuracy of 11 significant digits ($\mu_{pe} \simeq 1836.152673426(32)$ according to the NIST CoData project [6]), the LKB project aims to increase this accuracy to 12 significant digits. The H_2^+ ion is a three-body system with two protons and one electron. Its use is due to its particular sensitivity to μ_{pe} . Indeed, the wavelength of its vibrational transitions varies with a strong dependence of the order of $\nu \propto \frac{1}{\sqrt{m_p/m_e}}$.

To study H_2^+ , we need to induce a transition between two specific energy levels [7]: $-21205.1133 \text{ cm}^{-1}$ and $-15035.7831 \text{ cm}^{-1}$ (figure 1). The corresponding photons must therefore oscillate at a frequency of 184.951866 THz or a wavelength of 1620,922 nm. To ensure the accuracy of this transition, it is crucial to eliminate relativistic effects (due to second order Doppler effect), which could alter the transition frequency by 5×10^{-10} [8]. This requires cooling the H_2^+ ions. Given the impossibility of cooling these ions directly by laser cooling techniques, we use sympathetic cooling via a Coulomb crystal formed of Be^+ ions [9]. The latter are chosen because, having a mass close to that of H_2^+ ions, they are efficient

for sympathetic cooling. The Be^+ ions are effectively slowed down by Doppler cooling. The ions are confined in a linear Paul trap [12], a technique developed in 1975 but implemented in 1978 thanks to the improved precision of tunable lasers [11,12]. Today, tunable solid-state lasers enable precise emission over wide bands. However, accuracy in excess of 1 kHz is required, which is still a challenge.

In this paper, we look at how to precisely control a laser using a frequency comb locked to REFIMEVE, an ultra-stable signal broadcasted by SYRTE. First, we'll introduce the laser and how it works. Then, we'll look at the particularities of its frequency. We'll then explain the experimental set-up used to control the laser's frequency, and finally present the results, which we'll discuss.

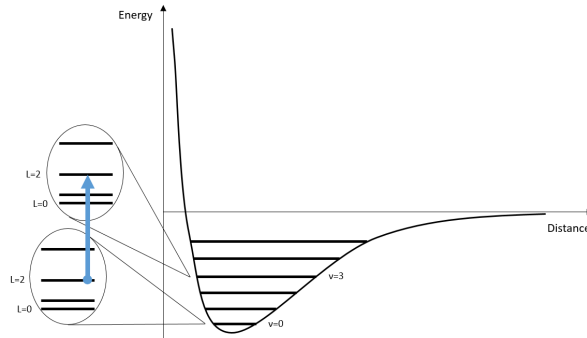


Figure 1: Interesting ro-vibrational transition in the fine structure of H_2^+ : $(\nu, L) = (0, 2) \rightarrow (3, 2)$.

2 Laser at 1621 nm

2.1 Introduction and Operation of the Laser

The studied laser is an infrared semiconductor laser developed and marketed by the brand TOPTICA Photonics [17]. This "Digital Laser pro" (hereafter referred to as DLpro) is paired with its controller, the "Digital Laser Controller pro" (DLC pro). In free-running mode at 20°C and under a maximum current through the diode, it emits at 1541.2 nm, which is still significantly distant from our target of 1621 nm.

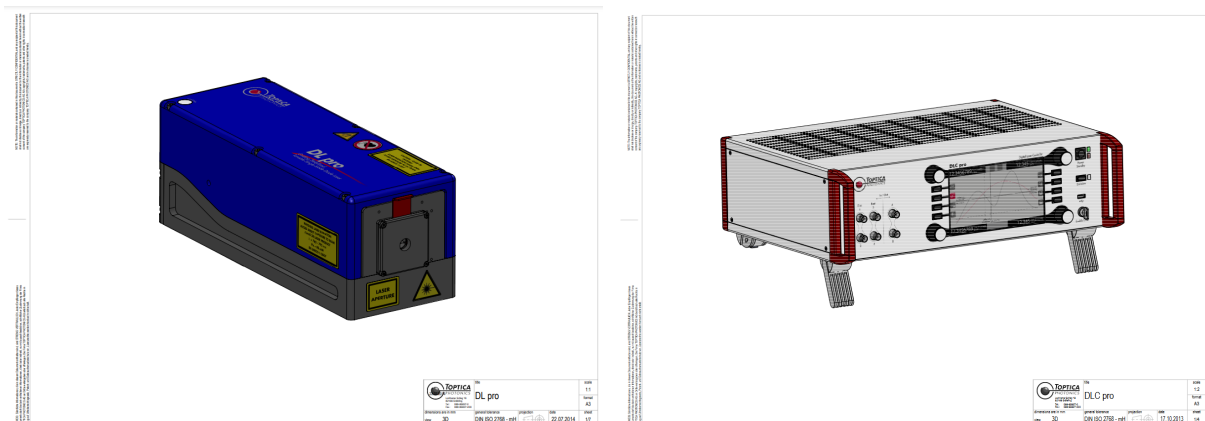


Figure 2: Technical drawings of the DLpro laser (Right) and the DLCpro controller (Left)

2.1.1 ECDL (External-cavity Diode LASER)

The laser under study belongs to the ECDL family. External-cavity diode lasers (ECDL) are tunable lasers that primarily use double-heterostructure diodes containing Gallium (Ga). The Fabry-Pérot cavity,

which enables the laser to operate, is, as the name suggests, external to the semiconductor material. The Fabry-Pérot cavity consists of:

- The laser diode: a semiconductor with one fully reflective wall (cleaved facet) and another wall treated with anti-reflection coating. Refractive indices close to 3 are commonly used in infrared devices, for example, Gallium Arsenide (GaAs) [14], Silicon (Si), or Germanium (Ge).
- A lens: this collimates the light beams emitted by the semiconductor.
- A diffraction grating: positioned in the Littrow configuration.

The Littrow configuration, shown in figure 3, is a method of orienting a diffraction grating in reflection mode [13].

The grating equation is recalled as follows:

$$\sin(\alpha) + \sin(\beta) = n \frac{\lambda}{a}, \quad (2.1)$$

where a is the grating spacing (interline distance); α the angle of incidence; β the diffraction angle (in the same direction as α); n the diffraction order and λ the wavelength of the incident light.

The Littrow configuration is a special geometry in which the incidence angle is chosen such that the diffraction angle β and the incidence angle α are identical. For a reflection grating, this means that the diffracted beam is retro-reflected in the direction of the incident beam. Therefore, in the Littrow configuration, we have $\alpha = \beta = \theta_L$.

Starting from equation (2.1), we obtain the Littrow position for $\alpha = \beta$:

$$\theta_L = \arcsin\left(\frac{n\lambda}{2a}\right). \quad (2.2)$$

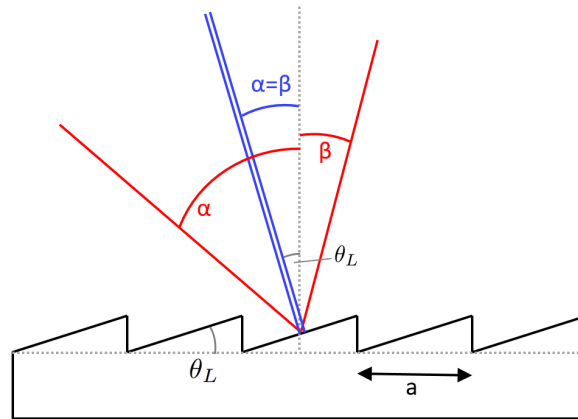


Figure 3: Reflection grating in Littrow position.

We do not have information about the characteristics of the laser diode, particularly its refractive index, nor about the characteristics of the grating.

The refractive index of the laser diode is useful for determining the reflection and transmission coefficients of the material (without the anti-reflection coating) using the formula:

$$R = \left(\frac{n_1 - n_2}{n_1 + n_2}\right)^2 \quad (2.3)$$

where n_1 and n_2 are the refractive indices inside and outside the semiconductor material. Since Gallium-based semiconductors typically have a refractive index of 3, we have $n_1 = 3$ and $n_2 = 1$, leading to : $R = \frac{4}{16} = 25\%$.

Next, the characteristics of the grating can be inferred from the laser's operation: the grating is positioned in such a way that it reflects the zeroth order towards the output and reflects the first order towards the semiconductor so that this beam is re-amplified.

For the n order of the network to be visible, there must exist an integer n such that $-1 \leq \sin(\beta) \leq 1$, hence, in Littrow's configuration: $-1 \leq -\frac{n\lambda}{2a} \leq 1$. So by reversal: $|n| \leq \frac{2a}{\lambda}$.

We want there to be only two orders of power distribution without loss between the Fabry-Pérot cavity and the laser output. So we only allow combinations of order $\{0;1\}$ or $\{-1;0\}$.

$$\begin{cases} |n| < 2 \Leftrightarrow b = \frac{1}{\lambda} > 616 \text{ grooves/mm} \\ |n| \geq 1 \Leftrightarrow b = \frac{q}{a} \leq 1234 \text{ grooves/mm} \end{cases}$$

To sum up, we need to respect the conditions $616 < b \leq 1234$ groove/mm to have an order of less than 2 in absolute value, and for there to be at least 1 order among $\{-1;1\}$. The usual industrial pitch values meeting these conditions are 900 and 1200 grooves/mm. If the network pitch is 900 (respectively 1200) grooves/mm, we check that the only orders present are indeed $\{0;1\}$. We also check that order 1 is only present if the angle of incidence is greater than 27° (respectively 70°).

In Littrow's position, the incident and 1st-order beams are perpendicular to the grating path. As a result, the grating is highly inclined to the incident beam at a pitch of 1200 grooves/mm.

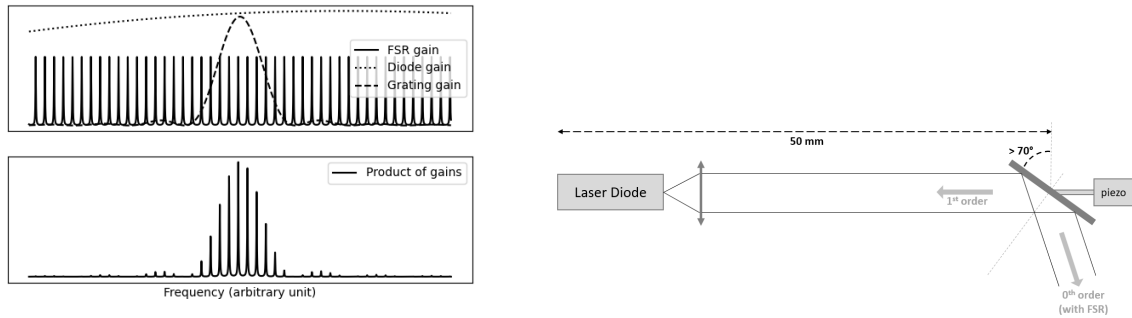


Figure 4: Left: Different gains responsible for the transmission frequency. (FSR: Free Spectral Range) Right: Grating positioning.

2.1.2 Laser control and control bandwidth

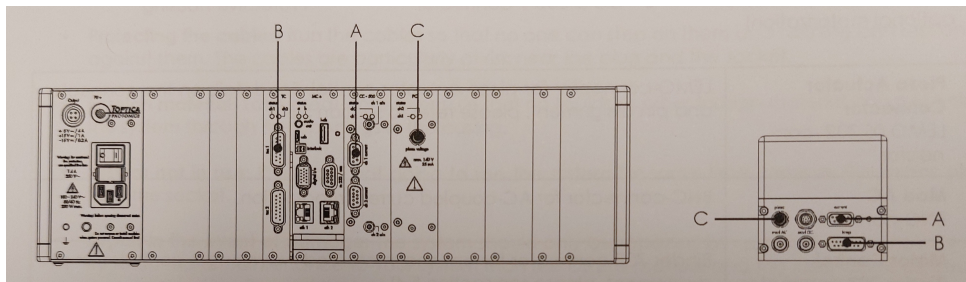


Figure 5: Connecting the DLpro to the DLCpro. A: Current control. B: Temperature control. C: Piezo-electrical device control.

The DLpro laser's natural wavelength can be modified over a wide band to achieve our objective. In this sense, it belongs to the family of tunable lasers. Several control parameters influence the wavelength. Firstly, the current I at the terminal of the semiconductor diode, which has a direct influence on the wavelength of the photons emitted. Secondly, the voltage U_{piezo} across the piezoelectric material controls the distance from the grating to the semiconductor. This varies the free spectral range (FSR) and therefore the wavelengths that can be lasered (figure 4). There could have been a second piezoelectric

ceramic controlling the rotation of the grating on itself, but our laser model doesn't have one. Finally, the temperature T of the medium in which the light evolves is stabilized by a PID loop in the laser.

As we'll see later in section (2.2.4), it's best to control laser intensity I . The DLpro can be tuned by different inputs on itself or on the DLC pro. To find out the control speed characteristics of these inputs, I sent a modulated signal through them [14]. Noting f_p and f_m as the carrier and modulation frequencies, modulating a signal $y(t) = A_p \cos(2\pi f_p t)$ results in a wave of the following type:

$$y(t) = A_p \cos(2\pi f_p t + \beta \sin(2\pi f_m t)). \quad (2.4)$$

In the complex domain, we have: $y(t) = \Re(\underline{y}(t))$ and $y(t) = A_p e^{i2\pi f_p t} \tilde{x}(t)$ with $\tilde{x}(t) = A_p \sum_{n=-\infty}^{+\infty} \underline{C}_n e^{i2\pi n f_m t}$ the Fourier series decomposition of $\underline{x}(t)$, a signal of period $\frac{1}{f_m}$.

This gives

$$\underline{y}(t) = A_p \sum_{n=-\infty}^{+\infty} \underline{C}_n e^{i2\pi(f_p + n f_m)t}. \quad (2.5)$$

The spectrum of $\underline{y}(t)$ contains the frequencies $f_p + n f_m$ that give the signal spectrum its characteristic side-band shape.

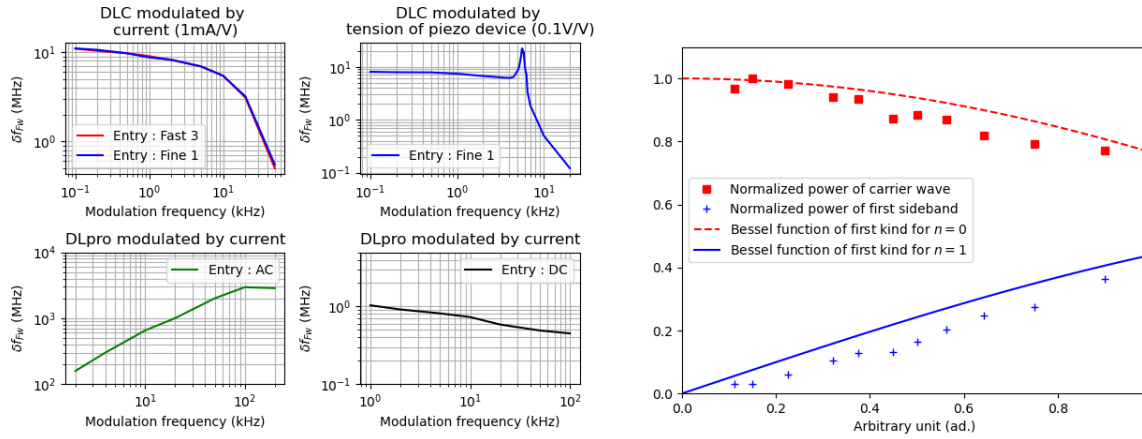


Figure 6: Left: Bandwidth display for different inputs. The input amplitude is set to 1V. Right: matching carrier and first side-band frequencies to first Bessel functions.

Noting, $J_n(\beta)$, the n^{th} Bessel function, we can then show that :

$$y(t) = A_p \sum_n J_n(\beta) \cos(2\pi(f_p + n f_m)t). \quad (2.6)$$

There are two equivalent ways of looking at this modulation: in phase (ϕ) or in instantaneous frequency ($\frac{1}{2\pi} \frac{d\phi}{dt}$). In both cases, the modulation depth is sought: β rad in phase and $f_m \beta$ Hz in frequency.

$$\phi = 2\pi f_p t + \beta \sin(2\pi f_m t) \quad \text{or} \quad \frac{d\phi}{dt} = 2\pi f_p + 2\pi f_m \beta \cos(2\pi f_m t) \quad (2.7)$$

On figure 6, we observe the different bandwidths and amplitudes of the modulation depth. Thus, the DLCpro entries, that command the DLpro with U_{piezo} , gives very fine but slow adjustment (cut-off frequency of 10 kHz). On the contrary, the DC entry on the DLpro, that commands I , gives fast and fine adjustment (no cut-off frequency). These considerations will be useful on the following pages.

2.2 Laser characterization

Having got to grips with the laser and its controls, I measured the laser's threshold current and power. Optical power is plotted as a function of control current, rather than electrical power, since the voltage

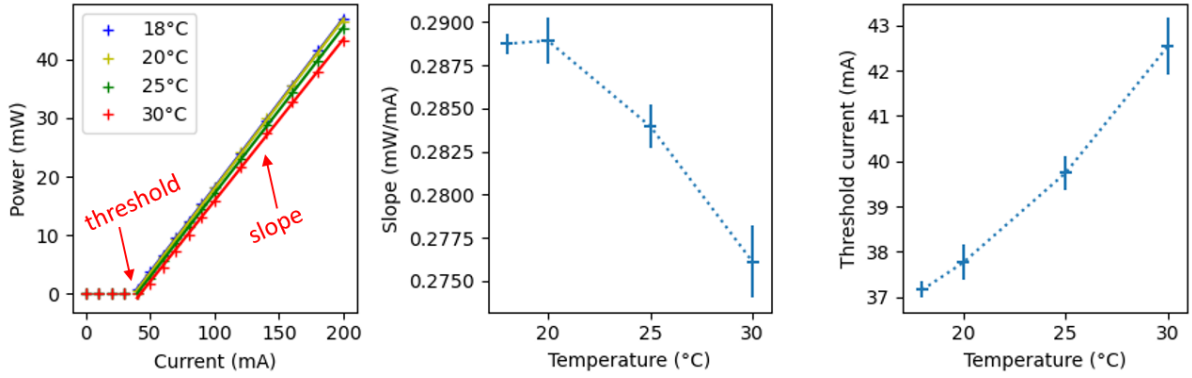


Figure 7: Left: I-P characteristic. Center and Right: Variable evolution with temperature. Powermeter: Gentec-e XLP12-3S-H2-D0 (offset of $\sim 15\mu\text{W}$)

across the laser diode is constant. This results in two additional curves giving the slope of the I-P characteristic and the threshold current as a function of temperature.

Temperature variations cause large deviations. Although the DLpro has a PID temperature controller, it is important to ensure a stable temperature environment around the laser. According to the manufacturer, the threshold for the laser to lase is 38.0 mA. This value is found to within 0.5% by measurement at 20°C. This deviation increases to 12.1% for 30°C. As for the slope of the characteristic, we also find the value of 0.29W/A announced by the manufacturer to within 0.3% for 20°C. This difference increases to 5.2% for 30°C (figure 7).

2.2.1 Gaussian beam

The laser propagates in space according to its wave equations:

$$\nabla^2 \mathbf{u} + k^2 \mathbf{u} = 0. \quad (2.8)$$

By injecting a wave of the type $\mathbf{u} = \epsilon \psi(x, y, z) e^{-ikt}$ with ϵ the polarization vector, we obtain the Gaussian field expression [15]:

$$u(r, z) = \frac{w_0}{w} \cdot \exp\left\{-i(kz - \phi) - r^2 \left(\frac{1}{w^2} + \frac{ik}{2R}\right)\right\}. \quad (2.9)$$

The associate intensity is

$$|u(r, z)|^2 = \frac{w_0^2}{w^2} e^{-\frac{r^2}{\left(\frac{w}{\sqrt{2}}\right)^2}}. \quad (2.10)$$

with $w(z)$ the waist in z : the diameter of the Gaussian beam, w_0 the waist at the origin, $R(z)$ the radius of curvature of the equiphase plane in $(r, z) = (0, z)$ and $\phi = \arctan\left(\frac{\lambda z}{\pi w_0^2}\right)$.

To check that the DLpro laser beam corresponds to the one expected according to theory, we set up an experiment in which we measure the laser's optical power while gradually obstructing the laser beam with a razor blade and a micrometer precision screw. By transit, we obtain what appears to be the prime of a Gaussian. To verify this, we try to approximate the curve to a sigmoid trend using the python library *scipy.optimize*. We can approximate the curves to this function with a coefficient $R^2 > 0.9999$:

$$f(x) = \frac{A}{2} \left[1 - \operatorname{erf}\left(\frac{x - \mu}{\epsilon}\right)\right] + \text{offset}. \quad (2.11)$$

What we're really interested in is the size of the beam's waist. Since we can't be sure of being at $w = w_0$, we assume that its size doesn't vary between the cavity and the measurement location. Noting σ the standard deviation of the corresponding Gaussian :

$$\begin{cases} \epsilon = \sigma\sqrt{2} \\ \sigma = -1/2w \end{cases} \Rightarrow |w| = \sqrt{2}\epsilon \quad (2.12)$$

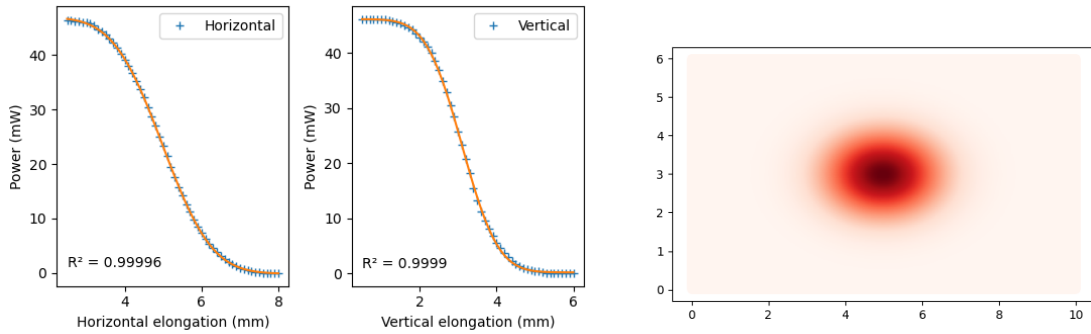


Figure 8: Gaussian beam profile. Left: Transit method. Right: cross-section reconstruction. (Temperature: 20°C. Intensity: 200 mA. Power: 46,4 mW.)

The beam is therefore an ellipsoid with axis lengths of 2.02 mm and 1.47 mm (figure 8). From the horizontal size of the beam, we deduce that for a 900 grooves/mm pitch grating, the beam covers 1286 grating features: $900 \times \frac{2.02}{2 \cos(45)} = 1286$ (inclined by 45°). Or, for a 1200 grooves/mm pitch grating, the beam covers around 1600 grating lines: $1200 \times \frac{2.02}{2 \cos(80)} = 6980$ (inclined by 80°).

The number of lines covered by the beam is important in determining the width of the grating's diffraction function (dotted line figure 4). It should be compared with the FSR (Free Spectral Range) of the cavity to determine how many peaks are likely to be lasered. A large number of preferential peaks will lead to a issue: mode hopping.

2.2.2 Free-running stability

The next step was to measure the laser frequency. To do this, we installed a mirror system that sends the laser beam into a wavemeter. The wavemeter chosen was the Bristol Instrument reference 671. After recording the frequency for almost three days, I could observe on figure 9 a drift in this frequency (left middle curve). This drift may be due as much to the DLpro laser as to the Bristol measuring instrument itself. To verify this, we use the ultra-stable 194400008.5 MHz REFIMEVE laser source from the SYRTE laboratory in Paris. A much smaller amplitude drift is observed (left bottom curve).

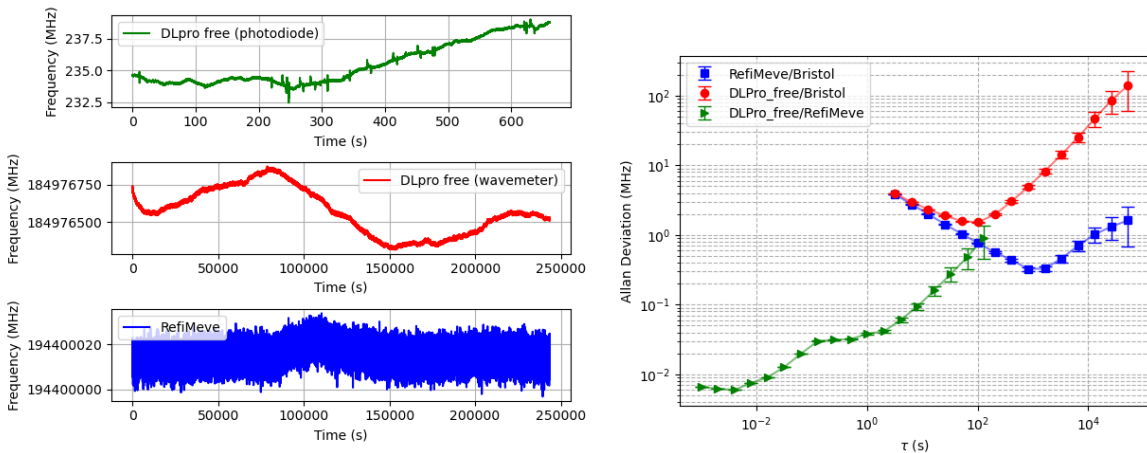


Figure 9: Time drift and allan deviation for DLpro and Refimeve measured with the Bristol wavemeter (Red and Blue) and for DLpro measured with a photodiode (Green).

To characterize these drifts, we calculate the Allan deviation. Given a time series $x(t)$ of measurement of a fluctuating quantity, the Allan variance is defined as :

$$\sigma_y^2(\tau) = \left\langle (\bar{y}_{n+1} - \bar{y}_n)^2 \right\rangle, \quad (2.13)$$

with \bar{y}_n defined as :

$$\bar{y}_n = \frac{x(n\tau + \tau) - x(n\tau)}{\tau}. \quad (2.14)$$

Finally, the Allan deviation (calculated by the *adev* function in the *allantools* python library) is given by :

$$\sigma_y(\tau) = \sqrt{\sigma_y^2(\tau)}. \quad (2.15)$$

We can see that REFIMEVE is more stable than DLpro in terms of frequency (figure 9). But it seems that for a τ of the order of an hour, the measurement is disturbed by the measuring instrument itself. So we decided to record the beat frequency between the DLpro and the REFIMEVE reference using a photodiode, in order to calculate the Allan variance more precisely over a short time. We can see that the two DLpro measurement curves coincide for $\tau > 100$ s.

We see a deviation for 2000 s of 180 MHz. So we're drifting by about 1 second every 10 days.

$$\frac{\delta\nu}{\nu} = \frac{180 \text{ MHz}}{184 \text{ THz}} \simeq 10^{-6}$$

2.2.3 Switch-on repeatability

To find out what the frequency is when the laser is switched off and then on again, I measured the frequencies for 20 successive switch-ons. The switch-on frequency is repeatable, within 300 MHz, with a deviation of 80 MHz (figure 10).

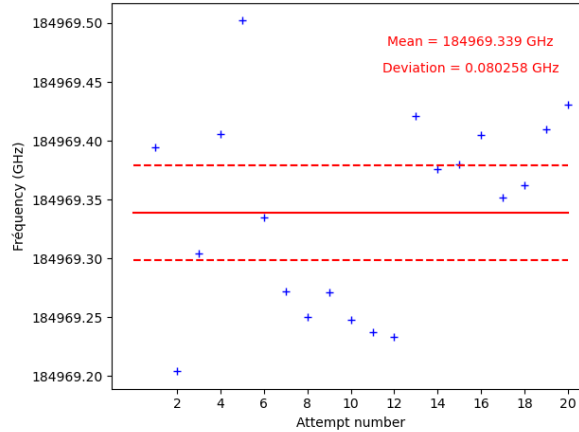


Figure 10: Visualization of average and variance of switch-on frequencies. The deviation is about 80 MHz. (Operating point: $I = 210$ mA, $T = 20^\circ\text{C}$ and $U_{piezo} = 70\text{V}$).

2.2.4 Possible control terminals and frequency ranges

The DLpro laser is a tunable laser, which means that its emission frequency can be varied over a significant range. To get an idea of the range, I performed measurements for all parameters. By varying the diode terminal current from 40 to 210 mA, the piezoelectrical controller voltage from 10 to 140 V and the temperature from 18 to 30°C , we obtain (figure 11) a frequency variation ranging from 184.93634 to 184.99702 THz (i.e. between 1620,526 and 1621,126 nm).

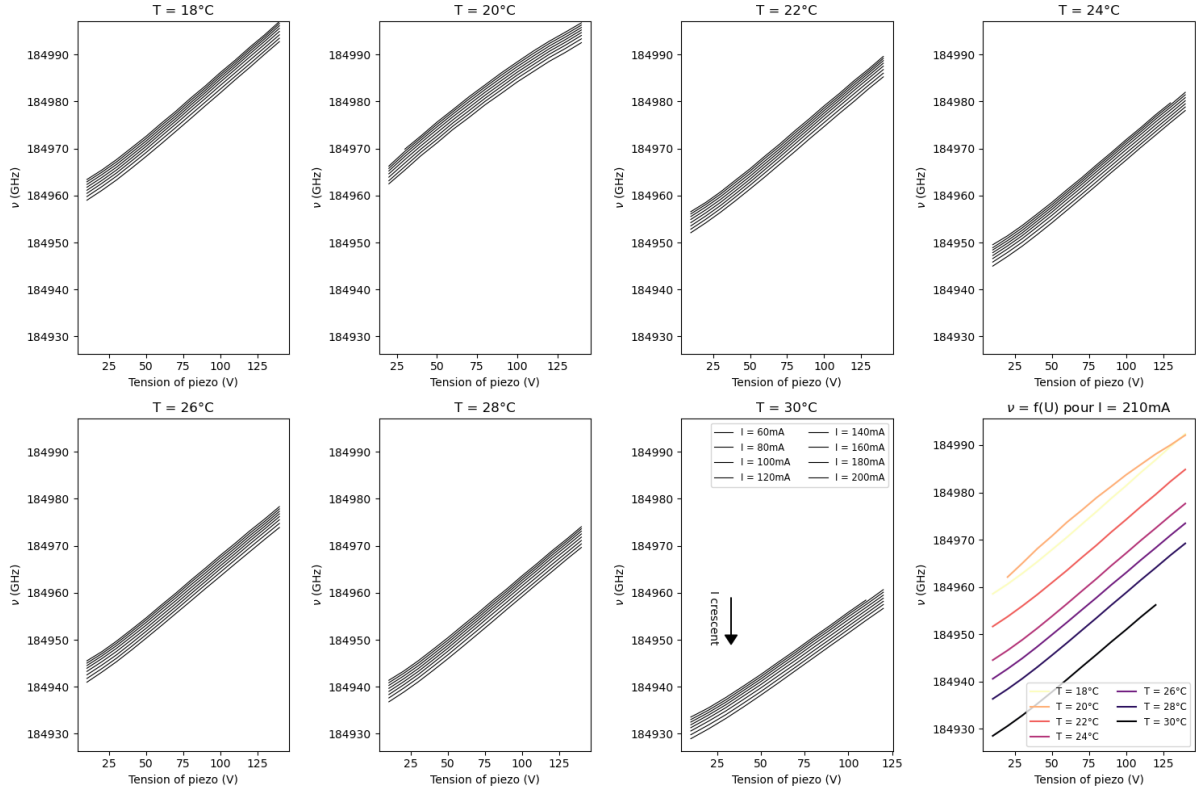


Figure 11: Frequency bounds on the range of all variables. ν has been traced by U_{piezo} for different I and T . For ν , function of U_{piezo} for different T , I took $I = 210$ mA.

We can see that frequency is a decreasing function of current, an increasing function of voltage and a decreasing function of temperature. In addition, setting the temperature or the voltage at the terminals of the piezoelectric device can give too coarse a setting. It is therefore preferable to drive the laser in intensity I to obtain a fine adjustment, after having set U_{piezo} and T roughly.

2.2.5 Hysteresis effect

Since laser frequencies can be varied over a wide frequency range, and the system is subject to many non-linearities, such as the laser diode, which is governed by non-linear optics, or piezoelectric devices, the frequency is subject to hysteresis. On figure 12, there is an example of hysteresis produced by varying U_{piezo} , the variable that enables fine tuning of the frequency.

As we can see on figure 12, if we vary the voltage in both directions by 20 V, trying to do little steps to avoid mode jumps, we find a hysteresis of 128 MHz. This is not insignificant.

3 Laser frequency control

In this experiment, we observe the beating phenomenon between the DLpro laser at 1621nm and a frequency comb. The idea is to control the laser frequency to observe the H_2^+ ion transition. We use a photodiode, which is more precise than an optical wavemeter. As a reminder, beating is obtained when two light sources of close frequencies are mixed. A coupling term then appears. If the two signals are $E_l = \epsilon E_l^0 e^{i(\omega_l t - \mathbf{k} \cdot \mathbf{r}) + \varphi_l}$ with $l \in \{1, 2\}$ and $E^0 \in \mathbf{R}$, then the intensity I of the photodiode is proportional to $|E|^2$, and in $r = 0$ (where the detector is located):

$$|E|^2 = (E_1^0)^2 + (E_2^0)^2 + E_1^0 E_2^0 \cos((\omega_1 - \omega_2)t + \varphi_1 - \varphi_2) \quad (3.1)$$

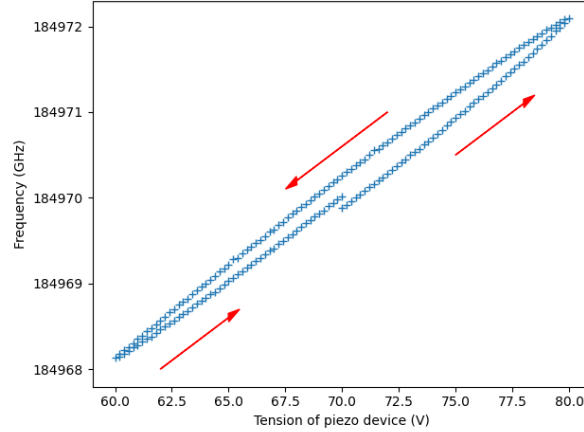


Figure 12: Frequency differences when returning to the same operating point in the presence of hysteresis. (Operating point: $I = 210$ mA and $T = 20^\circ\text{C}$.)

If we assume that comb frequencies don't fluctuate (as long as it's locked to REVIMEVE, this is almost true), beat control is equivalent to laser frequency control.

3.1 Protocol

3.1.1 Equipment

In this experiment, we'll be using our DLpro laser at 1621nm, a frequency comb, a fiber coupler, a photodiode, a phase comparator, a P-I corrector, a bandpass filter, a spectrum analyzer and a synthesizer.

3.1.2 Frequency comb

The LKB has a frequency comb [16], which is a laser source that emits a regular succession of very short pulses. In the frequency domain, the spectrum is a comb of teeth spaced f_{rep} apart. A comb with N teeth is equivalent to N continuous lasers of frequency equidistant from f_{rep} . The comb takes its name from this frequency distribution: $pf_{rep} + f_c$ with $p \in \llbracket -N/2, N/2 \rrbracket$ ($f_c = \omega_c/2\pi$ is the central frequency of the comb). Its electric field is given by :

$$\mathbf{E}(\mathbf{r}, t) = \mathbf{e} \sum_{p=-\frac{N}{2}}^{\frac{N}{2}} E_p e^{i((\omega_c + p\omega_{rep})t + \mathbf{k}_p \cdot \mathbf{r} - \phi_p)}, \quad (3.2)$$

with $\omega_{rep} = 2\pi f_{rep}$; \mathbf{k}_p the wave vector of tooth p ; \mathbf{r} the position in space; E_p and ϕ_p the amplitude and phase for each mode. In the ideal case, $\forall p \in \llbracket -N/2, N/2 \rrbracket, E_p = E_0; \phi_p = 0$, we obtain :

$$\mathbf{E}(\mathbf{r}, t) = \mathbf{e} E_0 e^{i\omega_0 t} \frac{\sin((N+1)\omega_{rep}t/2)}{\sin(\omega_{rep}t/2)}, \quad (3.3)$$

and then,

$$I \propto \|\mathbf{E}\|^2 \propto \left(\frac{\sin((N+1)\omega_{rep}t/2)}{\sin(\omega_{rep}t/2)} \right)^2. \quad (3.4)$$

In our frequency comb [16], ω_c is such that $\lambda_c \simeq 1,56 \mu\text{m}$, the frequency of oscillations in a pulse: $T_{\text{optical}} = \frac{1}{f_0} \approx \frac{1}{2.10^{14}} \approx 5\text{fs}$ and the time between two pulses: $T_{rep} = \frac{1}{f_{rep}} \approx \frac{1}{2.10^8} \approx 5.10^{-9}\text{fs} = 5\text{ns}$ (figure 13).

We can then lock it onto the REFIMEVE signal whose frequency is $f_{\text{REFIMEVE}} = 194\,400\,008\,500\,000 \pm 2$ Hz, id. $\lambda_{\text{REFIMEVE}} \simeq 1,542 \mu\text{m}$

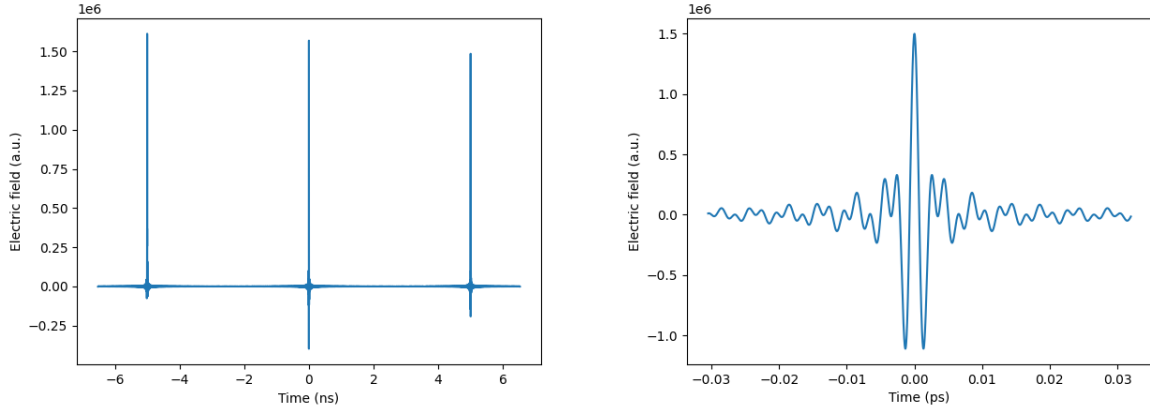


Figure 13: Left: Intensity of the comb in the ideal case. Right: Zoom on the central peak. ($T_{rep} = 5$ ns, $T_{optical} = 5$ fs, $p = 1,5 \times 10^6$)

3.1.3 Fiber coupler

With well-chosen comb characteristic values: $\lambda_c = 1,56 \mu m$, $f_{rep} = 200$ MHz and millions of p , we are sure to get a tooth close to our target value: 1621 nm.

As the two frequencies are close, we can beat. Taking the beat-note is useful because the frequency of the real wave is too high to be picked up directly by measuring instruments ($\lambda = 1621$ nm is equivalent to $\nu = 185$ THz). Performing the beat allows us to focus on the difference between two close frequencies, which greatly reduces the frequency of the signal we're interested in.

To achieve this, the comb and laser are injected into optical fibers using the empirical click-clac method. This method is useful for aligning the beam in the fiber according to the 4 degrees of freedom: two rotations around the vertical axis and two further rotations around the horizontal axis. The fibers we use are angled-cut to avoid reflexion to propagate back in the fibers. Noting n_{cl} and n_{co} refractive indices in cladding and core, the numerical aperture of the fiber is such that :

$$\sin(i_c) = \sqrt{n_{co}^2 - n_{cl}^2} \quad (3.5)$$

Once injected, these two fibers are connected to a 75/25 coupler (which means that 75% of the energy from the first source and 25% from the second are mixed through the device). We kept 75% of the comb power and 25% of the DLpro (because the comb was less powerful: $10.67 \mu W$ vs. $2,332$ mW).

3.1.4 Spectrum analyzer

After signal acquisition using a photo diode, the beat-note signal can be observed in a spectrum analyzer (figure 14). We can also use an attenuator upstream of the photodiode to avoid saturating it, and an amplifier downstream to detect the signal with the spectrum analyzer.

3.2 Results and improvements

On figure 15 left, numerous beats can be observed, some every 200 MHz, corresponding to the beating of the comb teeth against each other, and others in between for beats linked to the DLpro laser.

To select the beat we're interested in, I tuned the DLpro laser to emit at a frequency that gives a comb beat of about 240 MHz, then add a bandpass filter centered on 240 MHz to the device (figure 15 right). Then, to increase the signal-to-noise ratio, I needed to add a polarization controller between the laser and the fiber coupler. In fact, the intensity of the beat signal is proportional to the scalar product of the polarizations : $\epsilon_1 \cdot \epsilon_2$, which is optimized for $\epsilon_1 = \epsilon_2$.

This gives a signal-to-noise ratio (SNR) of 45 dB (in a 100 kHz analysis bandwidth).

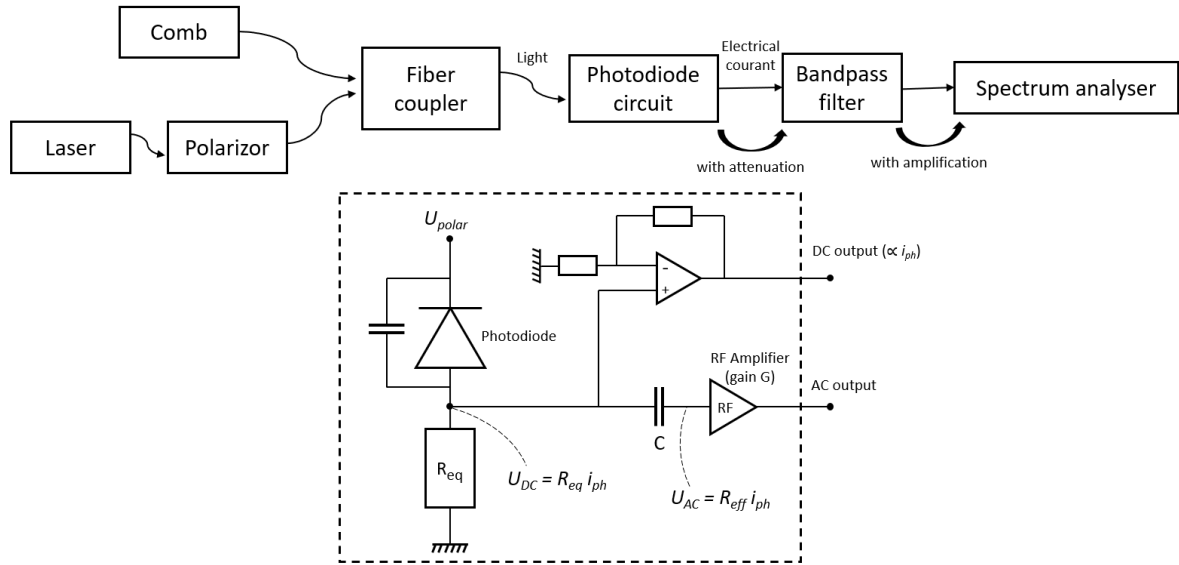


Figure 14: Top: Schema of mixing and analysis set-up. Fiber coupler: Koheron FOSPL12-7525. Spectrum analyser: Rigol DSA 815-TG. Bottom: Zoom on the photodiode circuit. We have $U(\omega) = R_{eq}(\omega)G(\omega)i_{ph}(\omega)$.

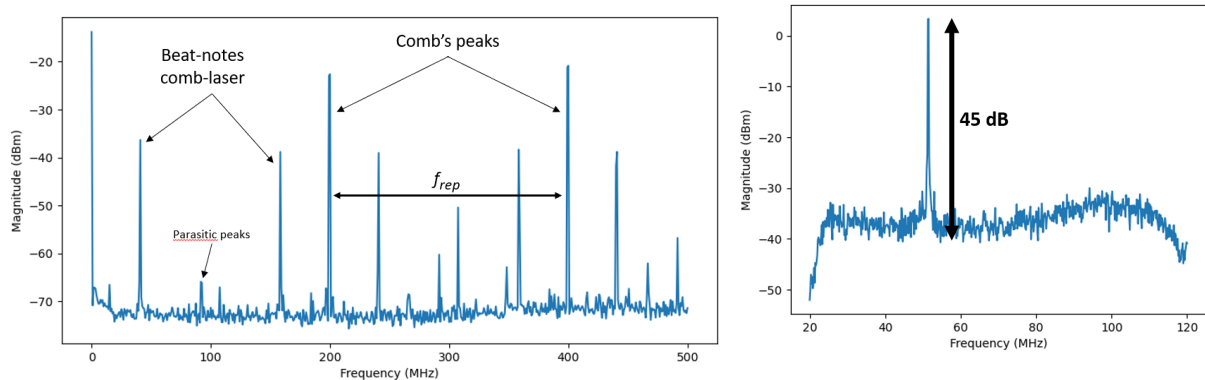


Figure 15: Left: Beat-note visualization before bandpass filtering (bandwidth 500 kHz). Right: After bandpass filtering (bandwidth 100 kHz). Comb's power: $11 \mu\text{W}$. Laser's power: 2, 3 mW.

3.3 Control

Now that we've isolated a peak from the beat signal using the bandpass filter, we can control the laser. To control the laser in frequency, we need to generate an error signal that depends on the distance from the true frequency to the desired frequency. This signal then passes through a feedback loop. The error signal is generated by a phase frequency detector (PFD). The PFD and the PI (Proportional - Integrator) are used in the phase lock loop (PLL).

3.3.1 Phase frequency Detector

In the PFD, we want to create a signal proportional to the phase difference between the two signals $s_1(t) = \sin(\omega_1 t + \varphi_1)$ and $s_2(t) = \sin(\omega_2 t + \varphi_2)$. One of these signals is the filtered beat-note of the laser with the comb. The other is a signal sent by a synthesizer that acts as a reference. We don't use its internal quartz crystal, but an external reference signal from the SYRTE laboratory, very accurate to 10 MHz.

The phase frequency detector's hardware consists of :

1. a component that transforms sinusoidal signals into square-wave signals.
2. a kind of “exclusive or” (XOR) gate that creates a new signal as a function of the other two.
3. a low-pass filter that acts as an averager with $f_c \ll \frac{1}{T} < \frac{\min(\omega_1, \omega_2)}{2\pi}$.

The signal in output of the XOR gate is 0 or 1 : $S \text{ XOR } S = 0$ and $S \text{ XOR } (\text{Not } S) = 1$. Therefore, the PFD output is therefore a number between 0 and 1, corresponding to the time average of the XOR output. There's a limit between 0 and 1, because every $2\pi[4\pi]$ the average jumps from 1 to 0. We then have three cases, depending on whether or not the counted signals oscillate at the same frequency.

- If $\omega_1 > \omega_2$ (respectively $\omega_1 < \omega_2$), then the mean is positive (respectively negative). As the frequencies are not the same, the phase drifts continuously and the observed triangles on the oscilloscope above 0 (respectively below 0).
- If $\omega_1 = \omega_2$ (figure 16), then the XOR of the two signals gives the phase difference between the two signals.

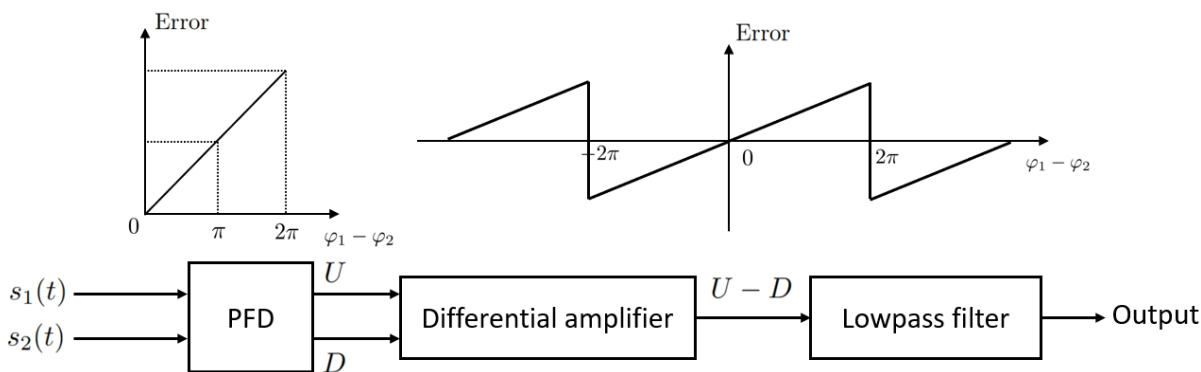


Figure 16: Left: Error signal created with a XOR gate. The unit of error signal is the percentage of the amplitude of the voltage of the square signal. Right: Output of the PFD set-up when $\omega_1 = \omega_2$. Bottom: Schema of the PFD set-up.

3.3.2 PI corrector and frequency control loop

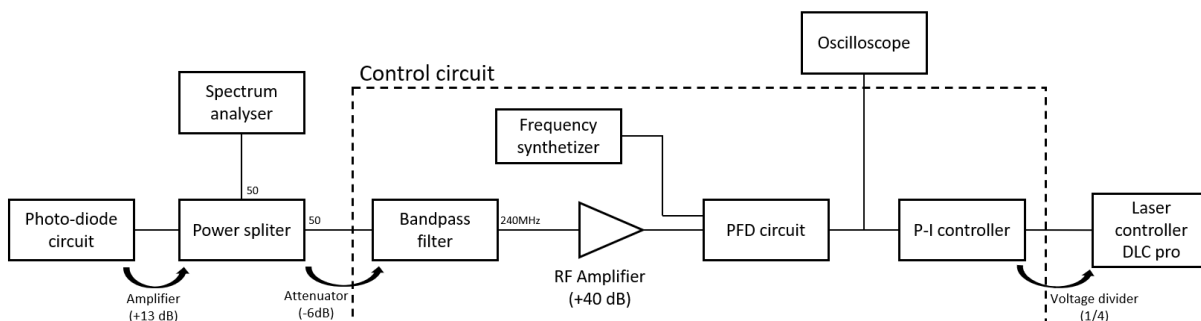


Figure 17: Overall schema of the control circuit. Power splitter 50/50: MiniCircuits ZX10-2-12-5. Tunable band-pass filter: Telonic Berkeley TTF 250-5-5EE. Oscilloscope: Tektronix TDS 1012. Amplifiers and attenuators : MiniCircuits devices.

To improve the lock, we introduce a proportional-integrator corrector between the PFD and the DLC pro. In reality, this is an $I'(P + I)$.

As we saw in sections 2.1.2 and 2.2.4, the modulation input on the DLC pro is rather slow and the DC input on the DLpro is rather fast. So we're going to use both inputs simultaneously. The I' has a small gain compared with the I : it is used to bring the laser frequency down to the target frequency. Then the $P + I$ with high gain takes over to lock in the frequency for good.

Once all the elements of the PLL have been assembled such as on figure 17, I have adjusted the PI gains to obtain the finest and largest peak possible. In effect, we're trying to get the best signal-to-noise ratio.

4 Results

4.1 Frequency and noise measurement

Once the free laser frequency is close to the target value, the lock can be applied. The result is a dirac spectrum centered on the target frequency. Two wings appear symmetrically on either side of the central peak. The noise has been driven out of the vicinity of the peak and spread further out.

Then I took several measurements which show that the signal obtained is composed of a sum of noise and the signal. We have the noise of the spectrum analyzer without inputs connected (in magenta); the noise of the photodiode without light (not shown); the noise of the photodiode with light, also known as shotnoise (in yellow); then we have the locked and unlocked signals (in blue and red respectively).

The signals are tangent to the shotnoise far from the peak.

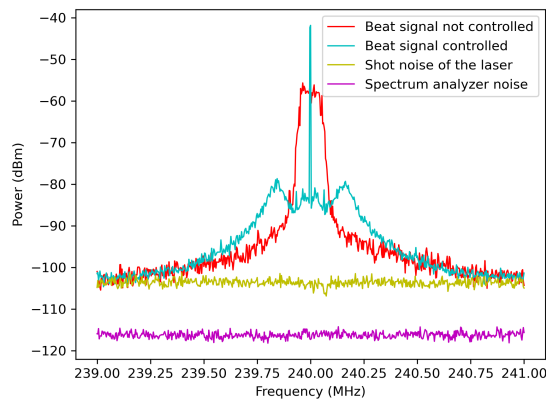


Figure 18: Frequency analyzer observation of different noise levels (magenta and yellow) and locked and unlocked signals (cyan and red) for a bandwidth of 2000 kHz.

4.2 Influence of PI

The proportional gain influences the speed of correction: we correct more or less for a given disturbance. The greatest possible P is therefore optimal. However, if the P is too high, oscillations will start, as excessive correction will cause the setpoint to be exceeded and the lock will be lost. The P must therefore be increased until such oscillations occur. On the spectrum (figure 19), increasing P deepens the frequency distribution in the vicinity of the central peak. This creates two wings of noise which obtain the power displaced from near the peak.

The integral gain influences persistent errors. If the error is non-zero for a long time, then the correction is amplified to bring the signal back to the setpoint. An I as large as possible cancels out persistent

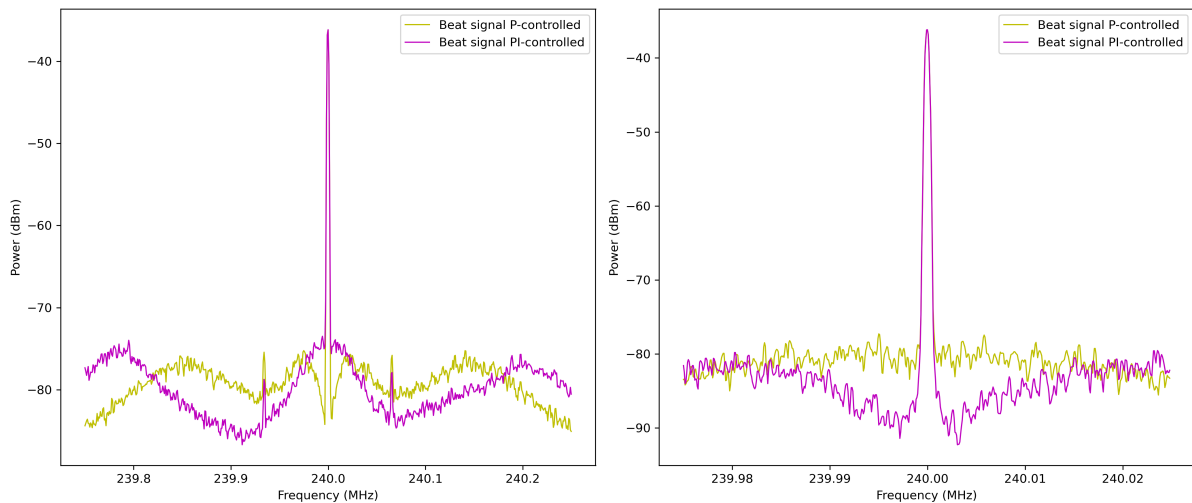


Figure 19: Influence of component change on beat-note with and without integrator for a bandwidth of 500kHz (left) and 50kHz (right).

errors and regime errors more quickly. But too high an I will cause oscillations, because, as with P, the correction can become excessive and cause overshoots that do not subside. On the spectrum (figure 19), increasing the I means moving the noise wings away from the central peak. This further increases the signal-to-noise ratio at the peak.

Here, after optimum adjustment of P and I, we manage to reduce noise in a bandwidth of 8kHz.

5 Discussion

5.1 Result limits

We found the right frequency, very accurate and precise. But this right frequency is not directly linked to a specific known command. In fact, it's only possible by cancelling the frequency error in the feedback loop. In addition, due to non-linearities in the semiconductor material, which cause a strong hysteresis phenomenon, the same command will not give the same frequency every time. This is also true during activation, when the semiconductor is in a transient regime, and the emitted wavelength varies for around ten seconds before stabilizing. This makes it impossible to know precisely (and without an external wavemeter) which tooth of the comb the laser uses to produce the beat signal when the laser is switched on. It also means that the laser frequency has to be pre-positioned near a tooth close to the target value before locking in, in order to lock in on the right tooth. Then, mode hopping is the bane of a stable laser. This doesn't really matter as long as the lock is working, but if you want to vary the commands quickly, the non-continuity of the wavelength with the commands raises issues. Finally, there is a kind of persistence in the laser mode. In theory, the laser lases for its highest gain, but once the laser has started lasing in one mode, that mode "eats" the available power through its own amplification. So a laser may not be in its preferential mode.

On the other hand, the speed of the feedback loop is very important. Indeed, the delay caused by a long calculation time can distort the correction if the error signal corrects a frequency that has already varied in the meantime. This phenomenon would favor oscillations close to equilibrium.

5.2 Improvement opportunities

To make sure the laser is in the right place, we'd need to establish a precise, repeatable start-up protocol that would ensure we end up at the right frequency on lightning. This protocol could include the following

instructions, among others:

- Before switching off the laser, return it to the operating point of interest (I, U_{piezo}, T) to avoid mode hopping, hysteresis or persistence on the next switch-on.
- Stabilize the temperature of the enclosure before switching on the laser.
- Switch on the laser and wait a few minutes for the emitting semiconductor diode to stabilize.

To address the problem of correction loop latency, we need to look at the hardware and connections. The first PI module contained a large number of low performance Integrated Linear Amplifiers, components which limit speed. We replaced them with better-quality components to speed up the circuit. The same applies to the components (resistors and capacitors) surrounding these ALIs : lowering the characteristic times of RC loops, present in integrators for example, increases circuit speed. We have $f_c = \frac{1}{2\pi RC}$ so lowering R or C increases bandwidth and response speed. Reducing delay in these ways would make it possible to increase P a little further without producing oscillation. The resulting peak in the spectrum would then be even finer and larger.

After improving ALI speed and reducing capacity values, here are the results:

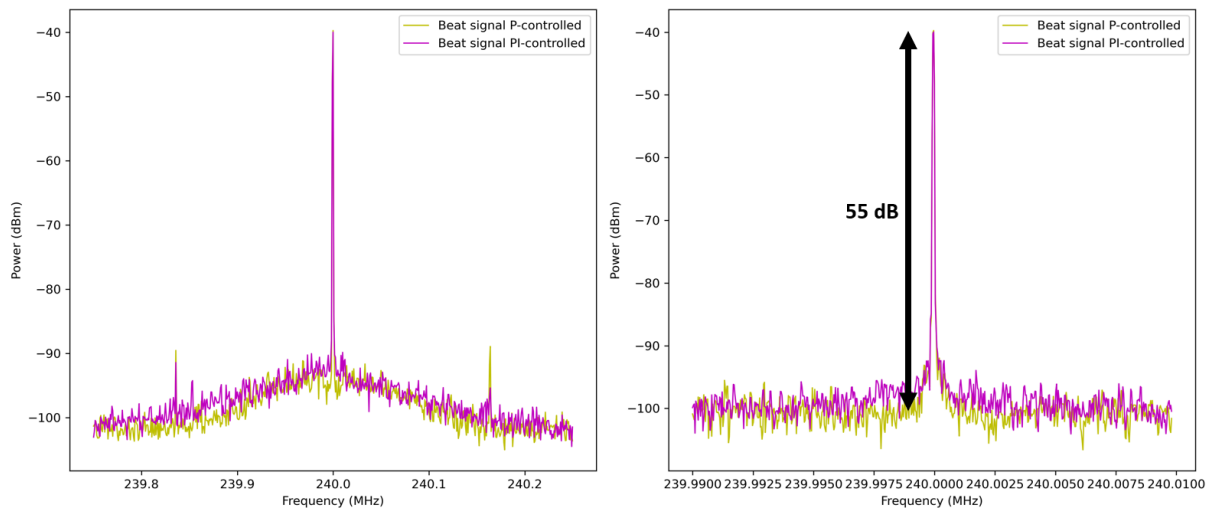


Figure 20: Influence of component change on beat-note with and without integrator for a bandwidth of 200kHz (left) and 20kHz (right).

We can see that the integrator of the PI no longer has much influence. This means that P is sufficient to apply a near-perfect correction. In fact, we increased P gain by a factor 4. The SNR ratio is now around 55 dB, that is a clear improvement.

6 Conclusion

This report explored the stabilization of a 1621 nm laser for precision spectroscopy of H_2^+ ions, a critical step in refining the measurement of the proton-to-electron mass ratio μ_{pe} . The laser system, based on an external-cavity diode laser (ECDL), was characterized for tunability and stability. Through analysis of power thresholds, temperature effects, and Gaussian beam profiles, the laser was shown to provide precise wavelength adjustments but displayed non-linear behaviors such as hysteresis. Free-running stability tests revealed minor drifts, while control parameters like diode current, piezoelectric voltage, and temperature offered complementary means of frequency tuning. To control it, a beat-note technique was employed to compare the laser output with a stabilized frequency comb locked to the REFIMEVE signal. The experimental setup utilized a photodiode, optical fibers, and a spectrum analyzer to isolate and analyze the beat-note signal. Phase-frequency detection and a proportional-integrative feedback loop allowed

precise locking to the target frequency. Fine-tuning the PI parameters reduced noise below 8 kHz, though challenges remained with mode-hopping and transient startup variability. While the current system demonstrates high precision and stability, improvements in repeatable startup protocols and hardware responsiveness are possible. These advancements will enhance the system's reliability and contribute to ongoing research on H_2^+ transitions and fundamental constants.

References

- [1] F. Heiße, F. Köhler-Langes & al. High-Precision Measurement of the Proton's Atomic Mass. *Physical Review Letters* 119. arXiv:1706.06780 [physics] (June 2017)
- [2] S. Sturm, F. Köhler & al. High-precision measurement of the atomic mass of the electron. *Nature* 509, 467-470. arXiv:1406.5590 [physics] (June 2014)
- [3] W.H. Wing, G.A. Ruff, W.E. Lamb, and J.J. Spezeski. Observation of the Infrared Spectrum of the Hydrogen Molecular Ion HD^+ . *Physical Review Letters* 36, 1488-1491. (June 1976)
- [4] L. Hilico, N. Billy, B. Grémaud & D. Delande. Polarisabilities, Light Shifts and Two-photon Transition Probabilities between $J=0$ states of the H_2^+ and D_2^+ Molecular Ions. *Journal of Physics B-Atomic Molecular and Optical Physics* 34. ISSN: 0953-4075 (Jan. 2001)
- [5] J.P. Karr, L. Hilico, J.C.J. Koelemeij, and V.I. Korobov. Hydrogen molecular ions for improved determination of fundamental constants. *Physical Review A* 94. (Nov. 2016)
- [6] P. Mohr, D. Newell, B. Taylor & E. Tiesinga, CODATA Recommended Values of the Fundamental Physical Constants: 2022. *Reviews of Modern Physics*. arXiv:2409.03787 [physics] (Sept. 2024) <https://physics.nist.gov/cuu/Constants/index.html>
- [7] R.E. Moss. Calculations for the vibration-rotation levels of H_2^+ in its ground and first excited electronic states *Molecular Physics* 80(6), 1541-1554. (Dec. 1993)
- [8] T. Louvradoux. Spectroscopie à haute résolution de H_2^+ : production et refroidissement sympathique d'ions piégés. *PhD thesis* Université Paris Cité (Dec. 2019)
- [9] J. Heinrich. Un piège à ions Be^+ pour la spectroscopie d' H_2^+ . *PhD thesis* Sorbonne Université (April 2018)
- [10] D.J. Wineland, R.E. Drullinger & F.L. Walls. Radiation-Pressure Cooling of Bound Resonant Absorbers. *Physical Review Letters* 40, 1639-1642. (June 1978)
- [11] T. Haensch & A.L. Schawlow. Cooling of gases by laser radiation. *Optics Communications* 13, 68-69. ISSN: 0030-4018 (Jan. 1975)
- [12] W. Paul, H.P. Reinhard & U.v. Zahn. Das elektrische Massensfilter als Massenspektrometer und Isotopentrenner. *Zeitschrift für Physik* 22, 365-368. ISSN: 1432-0630 (Aug. 1980)
- [13] A. Monmayrant, S. Auge & al. Wavelength Stabilized External Cavity Quantum Cascade Lasers using Cavity Resonator Integrated Grating Filters *IEEE*. hal-02447074 (Nov. 2019)
- [14] K. Petermann. Laser diode modulation and noise. *Kluwer Academic Publishers* Institut für Hochfrequenztechnik, Technische Universität Berlin (Nov. 2019)
- [15] H. Kogelnik AND T. Li. Laser Beams and Resonators. *PROCEEDINGS OF THE IEEE* 54, 1312-1329. (1966)
- [16] A. Mbaridi. Spectroscopie d'ions H_2^+ piégés : développement d'un laser à 9.17 μm référencé au système international d'unité. *PhD thesis* Sorbonne Université. tel-04523608 (Mar. 2023)
- [17] Toptica website (DLpro & DLCpro) : <https://www.toptica.com/products/tunable-diode-lasers/ecdl-dfb-lasers/dl-pro>